Caving 2026 – A van As, D Cumming-Potvin & J Wesseloo (eds)

doi:10.36487/ACG_repo/2645_23

Time-dependent convergence response of drawpoint pillars during undercutting and early caving at the Oyu Tolgoi Panel 0 block cave

Batbayar Batkhuu [a,*], Erkhembayar Enkhtaivan [a], Amarsanaa Biziyabal [a], Belgudei Batbayar [a], Lkhagvajav Tsogtbaatar [a]

[a] *Oyu Tolgoi, Rio Tinto, Mongolia*

Abstract

Extraction level instability is one of the main challenges in block cave mining, particularly in deep, high-column caves where drawpoint service life is extended until the ore column is fully exhausted. Oyu Tolgoi Panel 0 (OTP0) is one of the deepest block caving operations globally and is characterised by severe squeezing-type drawpoint failure resulting from highly faulted rock masses subjected to high in-situ stress and substantial column loading. This study investigates the time-dependent evolution of drawpoint damage at OTP0 using multiple deformation and convergence monitoring techniques. Continuous monitoring data are analysed to identify the progressive development of rock mass deformation and the primary mechanisms controlling drawpoint instability over time. The results reveal distinct deformation stages associated with key phases of the caving process, including undercutting, drawbell establishment, and cave propagation. These stages are governed by a combination of mining-induced stress redistribution, time-dependent rock mass behaviour, and geological controls such as faults and weak zones. The findings provide improved insight into the deformation mechanisms of highly deformable rock masses in block caving environments and support more informed strategies for undercut design, drawpoint management, and ground support planning in deep, high-stress caving operations.

Keywords: *block caving, convergence monitoring, time-dependent deformation, pillar damage*

1 Introduction

Block caving is increasingly being applied to mine large orebodies at significant depths, often exceeding 1 km below the surface. One of the key challenges in deep cave mines is maintaining stability at the extraction level (EXL) or extraction pillars, where high in-situ and mining-induced stresses can lead to deformation and failure. Typically, the EXL is developed only after the undercut has advanced past the area, reducing exposure to elevated abutment stresses. However, during the production or cave propagation phases, the EXL becomes more vulnerable due to higher extraction ratios and pre-existing stress-induced damage. At this stage, the dominant driver of instability is often the weight of the overlying cave material (cave loading), while the overall stress levels are relatively lower (Pierce 2018).

Oyu Tolgoi Panel 0 (OTP0) is one of the deepest operating block caves globally, where significant squeezing and closure have been observed, leading to drawpoint failures during the production stage. Notably, these failures have been localised in a specific area near the northern cave boundary and within the influence of major geological structures and weak zones. Understanding the mechanisms behind these failures and the key contributing factors is therefore essential.

* Corresponding author. Email address: batbayarbatk@ot.mn

This paper investigates the influence of operational, geological, and geotechnical factors on drawpoint pillar stability by leveraging an integrated dataset of geotechnical monitoring information.

Convergence measurements reveal that closure patterns evolve in distinct stages associated with undercutting, drawbell establishment, and cave propagation. The findings provide improved insight into the deformation mechanisms of highly deformable rock masses in block caving environments and support more informed strategies for undercut design, drawpoint management, and ground support planning in deep, high-stress caving operations.

1.1 Overview of Oyu Tolgoi Panel 0 caving

The Oyu Tolgoi (OT) operation is a world-class porphyry copper–gold deposit located in the South Gobi Desert of Umnugobi Province in Mongolia, approximately 550 km south of the capital city, Ulaanbaatar. The mine comprises several major orebodies, including Southern Oyu, Heruga, Hugo South, and Hugo North. Hugo North is the first orebody to be exploited using underground block caving and measures roughly 280 m in width, 2,000 m in strike length, and 600 m in vertical ore column height. It is developed in 2 lifts, with Lift 1 comprising 4 mining panels: P0, P1, P2N, and P2S (Figure 1).

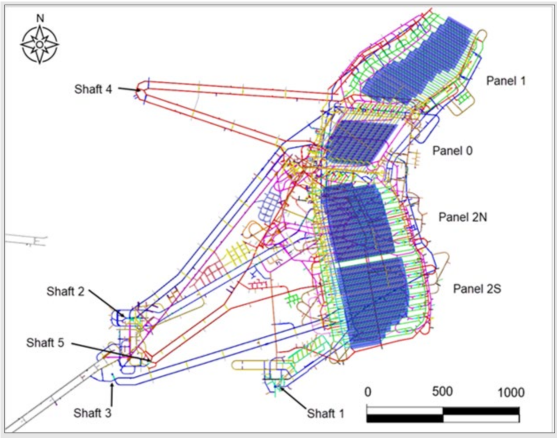

Figure 1 Hugo North Lift 1 mine design (Wooders et al. 2024)

The OTP0 is approximately 320 m in width and 280 m in length, developed with a production level at a depth of 1,300 m from the surface, employing an advanced undercut method with an apex level. P0 undercutting commenced in January 2022 and the last drawbell was fired in October 2024. Undercutting started from the weaker ground at the southwest corner of the footprint and was directed parallel to the major principal stresses. The El Teniente layout, with dimensions of 31 × 18 m, was implemented with a pillar thickness of 17 m between extraction and undercut levels. Figure 2 illustrates OTP0 footprint layout with sectional view of undercut sequence.

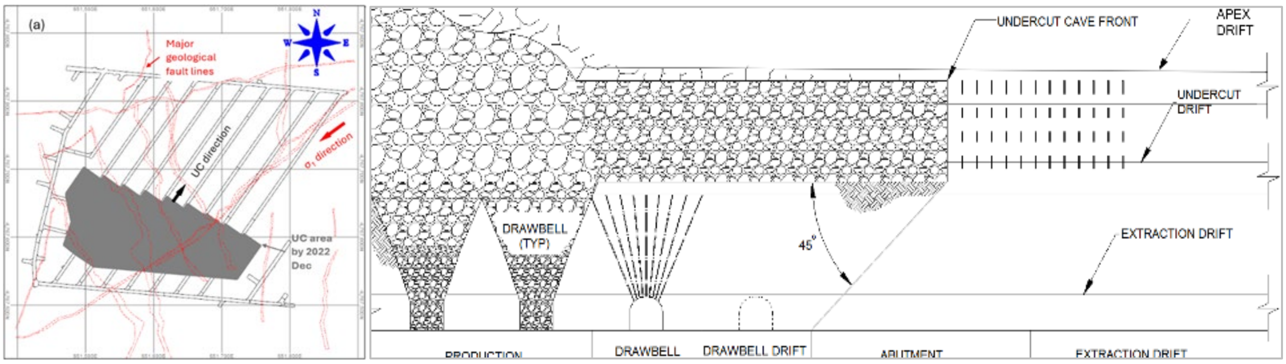

(a) (b)

Figure 2 (a) Oyu Tolgoi Panel 0 undercut level layout; (b) Section view along extraction drive illustrates undercut sequence

1.1.1 Geological setting and structural framework

The OT deposit is hosted within an easterly dipping, complex assemblage of Late Devonian to Early Carboniferous volcanic and volcaniclastic rocks. These units are intruded by multiple phases of porphyritic intrusions and overprinted by several generations of hydrothermal alteration (Crane & Kavalieris 2012).

Within the OTP0 footprint, the dominant lithological unit is quartz monzodiorite (QMD), which underlies the entire deposit area and hosts a significant portion of the copper–gold mineralisation. On the eastern side of the footprint, 2 main lithologies occur: massive porphyritic (augite) basalt (Va) and an intensely altered dacitic sequence, predominantly represented by ignimbrite (IGN). A post-mineralisation biotite granodiorite (BiGd) forms a northerly striking dyke complex composed of multiple sub-parallel to anastomosing dykes that cut through the western QMD intrusion and the overlying Va and IGN units. Figure 3 illustrates lithological units and structural features at OTP0 EXL.

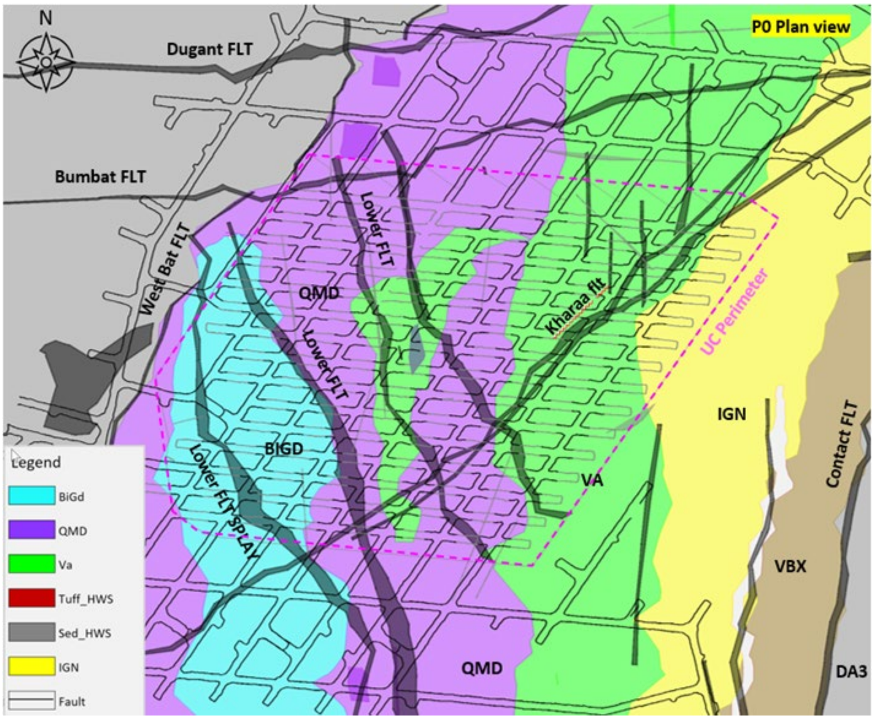

Figure 3 Plan view of lithology and major structural features at the Oyu Tolgoi Panel 0 extraction level

Structural architecture strongly influences the distribution of mineralisation, controlling both the original emplacement and the subsequent modification, displacement, and preservation of mineralised bodies during post-mineral deformation. Major structures in the Hugo North deposit are described by Porter (2016).

As shown in the Figure 3 , OTP0 is bounded by regional to major structures. On the western margin, the steep, near-vertical post-mineral West Bat Fault delineates the uplifted block hosting the Hugo North deposits. The West Bat Fault exhibits up to 1,500 m of vertical offset (west side down) and has undergone multiple episodes of movement; however, its total strike-slip displacement remains highly variable.

The northern boundary of OTP0 is defined by the east–west-striking, sub-vertical Bumbat Fault, a steeply dipping structure associated with variable dip directions in the Hugo North deposit. Several east–west faults like Dugant Fault offset both mineralisation and lithologies and display oblique-slip character.

The dominant internal structural feature within OTP0 is the Lower Fault system. This fault strikes north-northeast, dips moderately eastward, and cuts across the central to western portions of the footprint. It forms an intensely brecciated, clay gouge–rich zone. On the eastern side of OTP0, the east-northeast-striking Kharaa Fault crosscuts major lithological units and is interpreted as a reactivated structure associated with the regional Boundary Fault system.

Structural features, together with jointing and weak alteration infill such as clay and gouge, generate geotechnical domains with widely varying rock mass quality. Lower-quality domains are prone to severe squeezing under high stress. Therefore, geological structures represent a key driver of rock mass deformation and convergence in OTP0.

1.1.2 Geotechnical properties

The Hugo North area is situated within a tectonically strained environment, where in situ stresses are strongly influenced by regional compression and deep overburden. OT's stress regime does not follow a simple linear depth relationship. Instead, it reflects a combination of gravitational loading and a depth-independent tectonic strain component. As observed at similar geological settings such as the Canadian Shield, the stress field consists of a shallow stress-relief zone, a macrostructure-controlled transition zone, and a deeper tectonic strain-controlled zone (Ooi et al. 2022). The major principal stress (σ_1) trends approximately 54°, the intermediate stress (σ_2) is vertical, and the minor stress (σ_3) trends toward 144°. At the EXL depth near 1,300 m, σ_1, σ_2, and σ_3 are approximately 58, 34, and 27 MPa respectively, corresponding to a horizontal stress ratio ($K \approx 1.75$).

The geotechnical properties that govern the behaviour of the different geotechnical domains at OT are primarily lithology and alteration. Rock mass strength parameters were determined for each domain based on intact rock testing and face mapping data, particularly for in situ rock mass rating (IRMR) was determined using the classification system introduced by Jakubec & Laubscher (2000). Results emphasised the highly fractured nature of the Hugo North rock mass, particularly the intensity of the veining, which will serve to reduce the rock block strength. Table 1 outlines the intact rock mass properties compared against geological strength index values for dominant geotechnical units within P0 footprint.

Table 1 Intact rock properties from Ooi et al. (2022), and rock mass rating from Russo et al. (2023) of dominant lithologies for Panel 0

Lithology	Alteration	Intact rock properties					
		σ_{ci} (MPa)	m_i	σ_t (MPa)	E_i (Gpa)	GSI (RMR90)	IRMR (L&J2001)
BiGd	Unaltered (low vein density)	115.4	17.1	5.50	37.5	61	52
	Unaltered (high vein density)	80.4	17.4	3.80	33.3	58	49
QMD	Advanced argillic	55.7	16.0	2.80	63.1	55	45
	Intermediate argillic	78.4	19.4	3.50	57.8	59	42
	Phyllic (low vein density)	96.5	20.0	4.20	59.2	61	57
	Phyllic (high vein density)	108.8	15.8	5.50	59.2	60	52
	Potassic, propylitic	94.1	23.6	3.60	53.8	55	54
VA	Advanced argillic	72.2	10.0	3.1	59.7	60	57
	Intermediate argillic	72.2	19.0	3.1	56.7	60	57
IGN	Advanced argillic	77.5	10.0	5.10	62.2	60	54
FZ1	Weak fault zone	–	–	–	–	33	31
FZ2	Moderate cohesive fault zone	–	–	–	–	50	34

BiGd = biotite granodiorite; QMD = quartz monzodiorite; VA = porphyritic (augite) basalt; IGN = ignimbrite

P0 was expected to be affected by high abutment stresses induced during undercutting, followed by high column loading during the caving stage. The EXL excavations have experienced severe squeezing, particularly in areas within major geological structures and their associated damage zones. These conditions have contributed to localised instability, stress rotation, and block relaxation within the excavation footprint.

2 Methodology

At OTP0, highly fractured ground conditions combined with elevated stress levels contribute to progressive squeezing-type deformation.

Analysing convergence data is therefore essential for distinguishing between deformation resulting from:

- immediate stress redistribution (e.g. undercutting, drawpoint development, drawbell establishment, and cave propagation)
- longer-term, creep-like behaviour of the weak rock mass .

To assess time-dependent convergence, deformation monitoring data were integrated with local mining and geological information for each monitoring location. Convergence trends were evaluated by examining rate changes in relation to operational milestones, the presence of geological structures, and complementary monitoring data obtained from convergence stations and multi-point borehole extensometer (MPBX) instruments. This integrated assessment enables early identification of periods when deformation is likely to accelerate and instability may intensify.

2.1 Monitoring systems and integration of multiple data sources

At OTP0, a wide suite of monitoring technologies was deployed to track progressive drawpoint failure in a deep, high-stress, and geologically complex caving environment. Each monitoring method has unique temporal and spatial strengths; therefore, combining these datasets provides a more holistic understanding of rock mass behaviour. Figure 4 presents the monitoring systems deployed across the OTP0 footprint for acquiring and synchronising time-series deformation data, and their primary role and typical cadence.

Monitoring System	Function	Typical Cadence
Seismic system	C	Real-time
MPBX	A B C	Real-time
Visual damage mapping	A	Periodic (Weekly)
Tunnel borehole monitoring	A B C	Periodic (Quarterly)
3D Lidar and Mobile scanning	A	Periodic (Seldom)
Convergence pins	A	Weekly

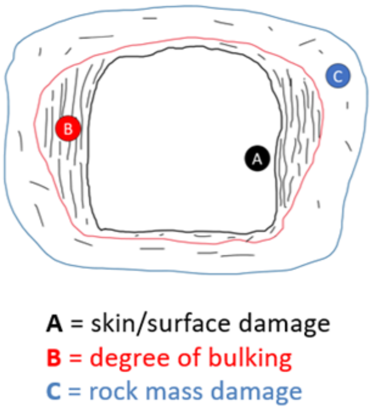

Figure 4 Key footprint level monitoring system at Oyu Tolgoi Panel 0 adopted from Ooi (2020)

Monitoring systems for assessing extraction-level stability at OTP0 were implemented in alignment with the advanced undercutting sequence, with the objective of capturing continuous deformation both before and after the undercut passed each area. The primary monitoring datasets used in this study are convergence and MPBX recordings, as these instruments were systematically installed and regularly measured to assess EXL pillar stability.

Convergence pins and horizontal MPBX instruments were installed in extraction drives at pillar locations between future drawpoints, which were mined following undercutting. At drawpoint intersections, only vertical MPBXs were installed to monitor rock mass displacement within the major apex pillar.

Both mining and geotechnical information are integrated into the Palantir Foundry platform to support data analysis and operational workflows (Moorcroft et al. 2022). Figure 5 illustrates the Palantir geotechnical excavation risk (GER) application dashboard for the P0 EXL and highlighting monitoring configuration for single EXL pillar.

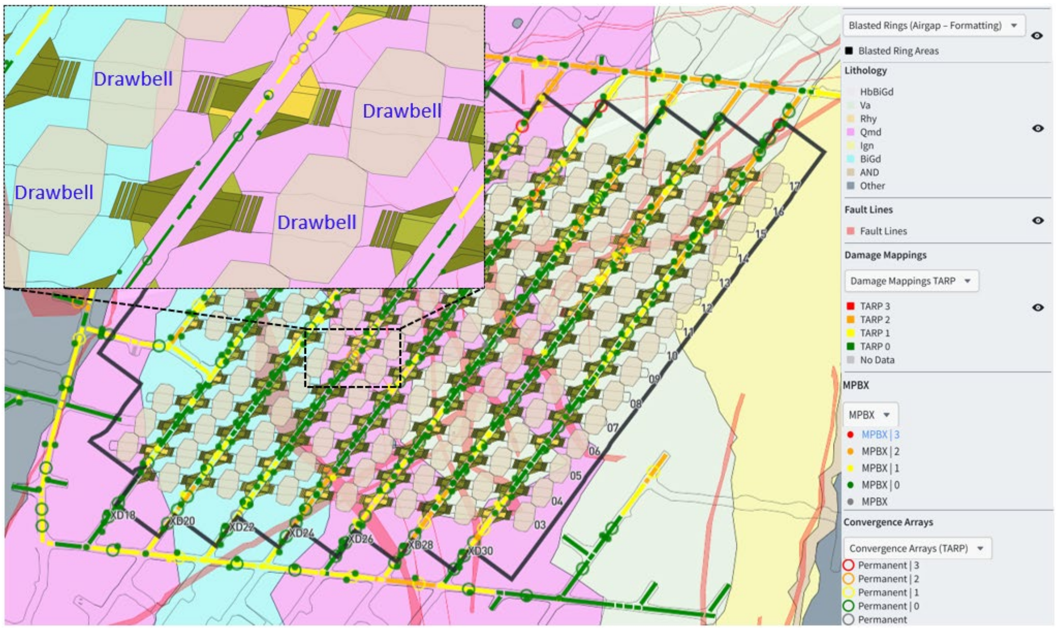

Figure 5 Geotechnical excavation risk dashboard highlighting convergence and multi-point borehole extensometer (MPBX) configurations for the drawpoint pillars

At OT, excavation reliability is enhanced and operational risks are mitigated using trigger action response plans (TARPs), which are based on defined levels of ground support deterioration and rock mass damage identified from single or multiple monitoring systems. Excavation condition is assessed through a combination of visual observations and geotechnical monitoring data and is categorised into 4 damage levels. Each monitoring method has its own unique set of TARP thresholds which correspond to excavation risk ratings. For convergence-based monitoring, the TARP levels at the OTP0 are defined as follows (Oyu Tolgoi 2025):

- Level 0 normal: normal excavation conditions where convergence behaviour and visual observations are acceptable and considered sustainable in the long term.
- Level 1 slight damage: minor damage to ground support, indicated by any of the following criteria:
  - cumulative convergence > 150 mm
  - MPBX displacement > 75 mm
  - convergence rate > 2 mm/day
  - MPBX displacement rate > 1 mm/day.
- Level 2 moderate damage: moderate damage to ground support, indicated by any of the following criteria:
  - cumulative convergence > 300 mm
  - MPBX displacement > 150 mm
  - convergence rate > 4 mm/day
  - MPBX displacement rate > 2 mm/day.
- Level 3 heavy damage: severe damage to ground support, indicated by any of the following criteria:
  - cumulative convergence ≥ 400 mm
  - MPBX displacement > 200 mm
  - convergence rate > 6 mm/day
  - MPBX displacement rate > 3 mm/day.

TARP-based monitoring provides a practical operational framework for identifying early signs of rock mass damage and implementing timely controls to prevent further deterioration. Because individual monitoring methods do not provide uniform spatial or temporal coverage, this study adopts a geospatial, pillar-based data integration approach. Monitoring instruments and mining activities located near each drawpoint pillar are spatially linked to that pillar, enabling a consistent and comprehensive assessment of local conditions. Figure 6 illustrates how monitoring data points, including MPBXs, convergence stations, undercut rings, drawpoints, and drawbell blasting locations, are mapped and integrated within the drawpoint pillar grid.

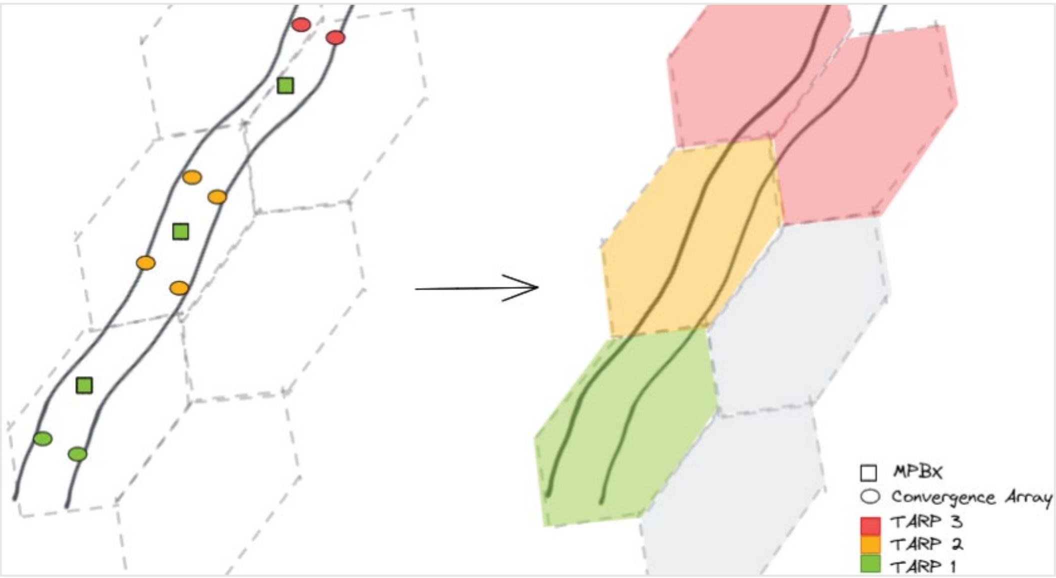

Figure 6 Mapping monitoring points into the drawpoint pillar grid (Moorcroft et al. 2022)

2.2 Convergence and time-series analysis

Time-series convergence analysis examines how deformation at the EXL tunnel evolves over time, rather than relying solely on cumulative displacement. The analysis in this study uses time-series data from horizontal MPBXs, vertical MPBXs, and convergence stations installed throughout OTP0.

Previous monitoring data analysis by Batkhuu & van As (2026) identified a consistent trend in convergence rate behaviour during undercutting, where both the rate and magnitude of convergence increased as the undercut expanded and concentrated around major fault zones. These findings highlight that exposure time and distance to elevated abutment stresses are critical contributing factors to rock mass damage. Building on these outcomes, the analytical framework applied in this study follows a similar process.

First, integrated pillar-scale monitoring data are grouped according to the major mining stages influencing deformation behaviour: pre-undercutting, post-undercutting, the pillar-forming stage, and the cave-propagation stage. Second, the grouped monitoring data are further classified by abutment time and rock mass condition, distinguishing between faulted and non-faulted ground.

Finally, visual comparison and correlation analyses are performed to examine differences in convergence behaviour across mining stages and rock mass classes. This approach enables evaluation of the relationships between deformation trends, operational activities, geological structures, and local stress conditions.

3 Results and discussion

A total of 98 horizontal MPBXs (into tunnel sidewalls), 47 vertical MPBXs (at drawpoint intersections), and 280 2-point (horizontal only) convergence stations were installed around drawpoint pillars across OTP0. Of these, 49 horizontal MPBXs (50%) and 18 vertical MPBXs (38%) produced continuous or near-continuous time-series spanning the undercut passage, pillar-forming stage, and early production. Only continuous MPBX data was used to cross-check convergence measurements.

For convergence monitoring, although nearly all pins required reinstallation at some point due to mechanical damage from mining activities, approximately 500 convergence pins were installed progressively over time, and the available readings could still be linked into continuous datasets. Consequently, convergence points are mapped onto a pillar-based grid defined by actual EXL pillars located between adjacent drawpoints, with grid dimensions of approximately 12–18 m. Figure 7 illustrates the grid-based linking of multiple convergence pin measurements collected over time within same pillar area.

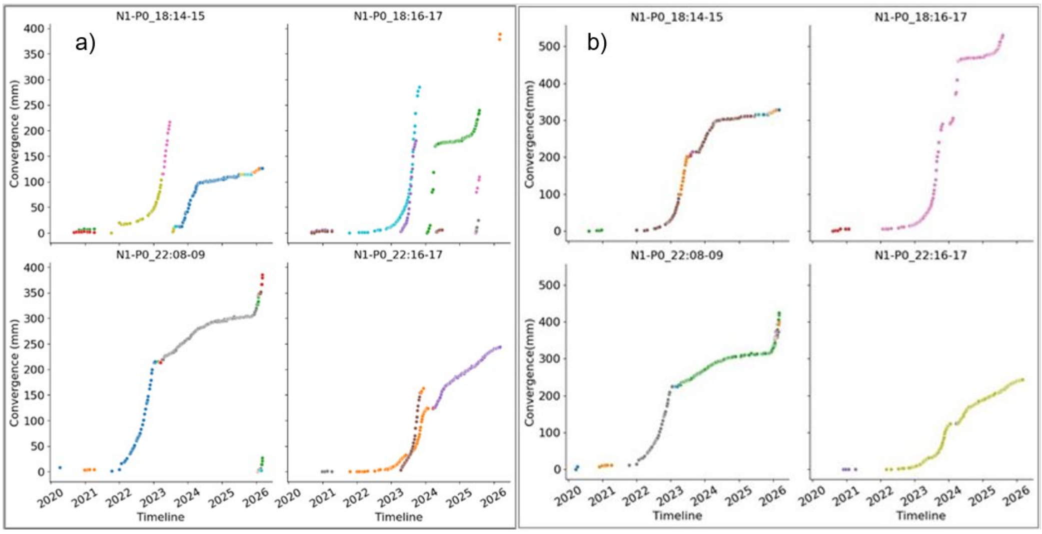

Figure 7 Linking of convergence measurements by pillar grid

Co-located horizontal MPBXs and convergence stations show close agreement in deformation patterns over time, with MPBX displacements exhibiting consistently smaller magnitudes, as expected, because MPBXs measure rock mass movement beyond approximately 0.5 m from the tunnel surface. This concordance between independent monitoring systems supports the robustness of the time-dependent convergence interpretations. Figure 8 presents an example of co-located horizontal MPBX and convergence measurements within the same pillar area.

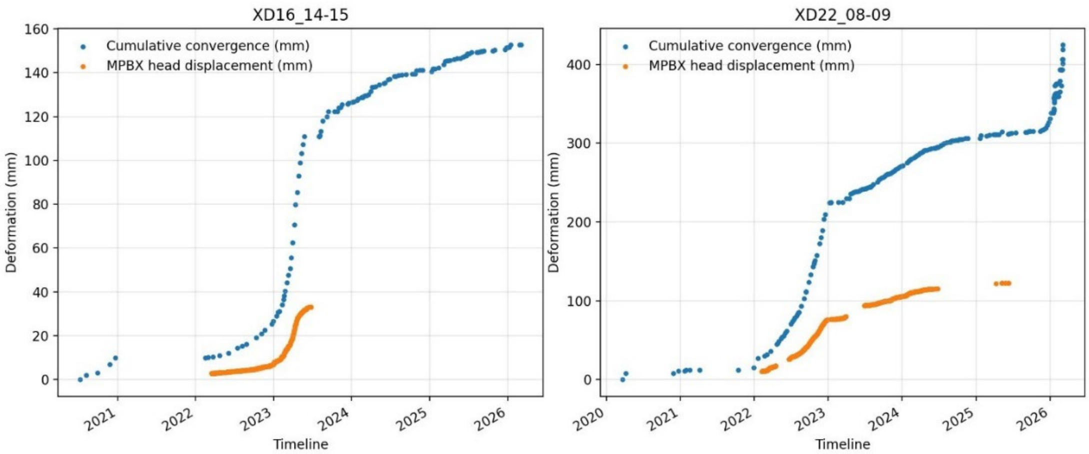

Figure 8 Two examples of drawpoint pillar of cross-plots comparing horizontal movement between instrument pairs

3.1 Stage-dependent behaviour and spatial concentration of convergence

Both MPBX and convergence datasets exhibited largely consistent deformation patterns. Most deformation occurred as the undercut passed above over the pillar locations, followed by a period of stabilisation until the pillar-forming stage. Based on this behaviour, the total convergence was divided into 2 primary components: the undercutting phase (up to the pillar-forming stage) and the early production phase.

During the undercut phase, cumulative convergence and peak convergence rates were increased as undercut expanded. This indicates that abutment stresses are highest immediately before and after the undercut passage and remain elevated as the undercut size increases. Superimposed on this operational control is a geological control: the zone is intersected by a Lower Fault splay and other fault associated weak/damaged zone.

Cumulative convergence values for each pillar during the undercut stage, at the point when the surrounding four drawbells were blasted and the EXL pillar was formed, are shown in Figure 9a. These results are compared with the hydraulic radius of the blasted UC area and superimposed with the major geological structures within the extraction footprint (Figure 9b).

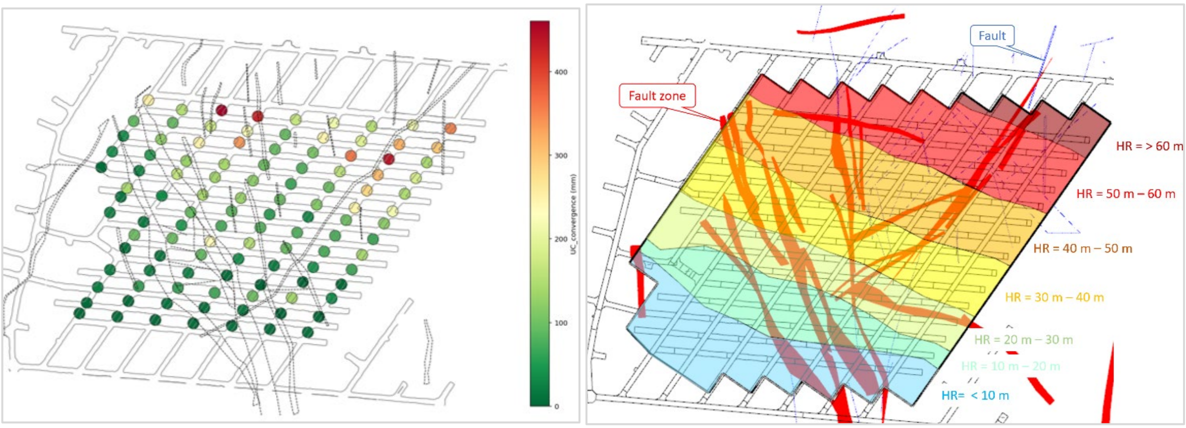

(a) (b)

Figure 9 (a) Cumulative convergence during undercut stage and (b) hydraulic radius zones by undercut advances overlain with geological structures at P0 extraction level

Convergence analysis covered the period from the onset of undercutting (UC) to 6 months after UC completion across the full footprint, beginning when the first severe DP pillar damage was observed in the northern section. Nearly 90% of the total convergence occurred during the UC stage for all zones, and at higher convergence rates. Following UC completion and pillar formation, deformation transitioned to a relatively slow, continuous rate across the extraction footprint. Cumulative deformation magnitudes and convergence rates during the undercutting and early production stages were subsequently compared, as summarised Table 2.

Table 2 Convergence summary by caving stages (undercutting and early production)

Drawpoint pillar group by undercut hydraulic radius	UC stage		Early production stage	
	Commutive convergence, mm	Convergence rate, mm/day	Commutive convergence, mm	Convergence rate, mm/day
HR < = 25 m	Max:136.9 Min:5.0 Average: 73.7	Max: 0.7 Min: 0.05 Average: 0.3	Max:137.6 Min: 10.3 Average: 79.3	Max: 0.07 Min: 0 Average: 0.03
25 m < HR < =50 m	Max: 235.7 Min: 41.1 Average: 124.6	Max: 1.2 Min: 0.2 Average: 0.7	Max: 260.65 Min: 80.5 Average: 139.5	Max: 0.27 Min: 0 Average: 0.08
HR > 50 m	Max: 460.9 Min: 95.9 Average: 241.6	Max: 2.3 Min: 0.4 Average: 1.2	Max: 603.7 Min: 101.1 Average: 293.9	Max: 1.3 Min: 0 Average: 0.3

3.1.1 Mechanistic synthesis for the northern boundary pillars

Localised drawpoint pillar damage observed during early production in extraction drives 18 and 20 (XD18 and XD20) is attributed to the combined effects of prolonged abutment exposure and inherent structural weakness. These damaged pillars are situated along the northern boundary of the footprint. Although convergence patterns and temporal trends during the UC stage are broadly consistent across all drawpoint pillars, the northern boundary pillars exhibited systematically higher cumulative convergence and convergence rates than those in the central and southern areas.

During undercutting, northern boundary pillars recorded a median cumulative convergence of 265 mm, with two pillars (XD18 and XD20), located within the Lower Fault zone, exceeding 400 mm (TARP Level 3). In contrast, central and southern pillars showed substantially lower deformation, with a median cumulative convergence of 100 mm; only two pillars within the Lower FLT zone exceeded 150 mm (TARP Level 1).

A similar contrast is evident in convergence rates as the UC front passed the pillar locations. Northern pillars exhibited a median convergence rate of 1.1 mm/day, with a peak of 2.1 mm/day recorded at XD18. Central and southern pillars showed lower rates, with a median of 0.5 mm/day and a peak of 1.2 mm/day.

In addition to elevated convergence rates during the UC stage across all northern boundary pillars, the 2 severely damaged pillars (XD18 and XD20) also experienced pronounced high-rate convergence during drawpoint mining and drawbell establishment (pillar-forming stage). Figure 10 presents the convergence histories of the northern boundary pillars plotted against time relative to UC completion.

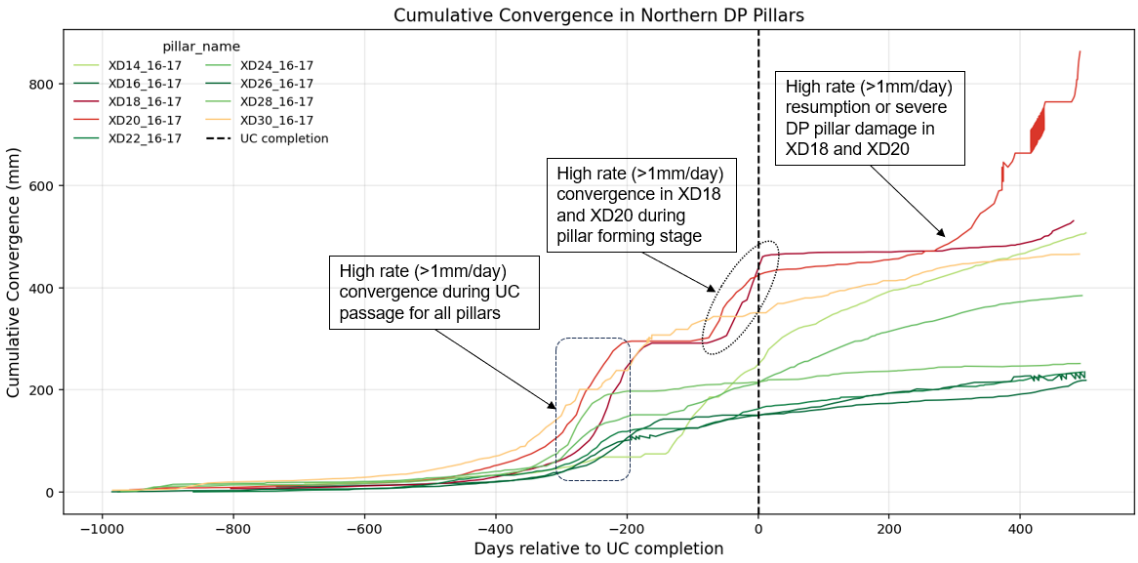

Figure 10 Time-series convergence of the northern pillars illustrating high-rate deformation during undercut passage, pillar formation, and onset production. Day 0 marker defines the undercut completion

The elevated convergence at the 2 DP pillars is primarily associated with their intersection with a Lower Fault splay zone, as there is no clear distinction in convergence rates along the northern boundary after UC completion, which remain consistently around 0.3–0.5 mm/day (Figure 11).

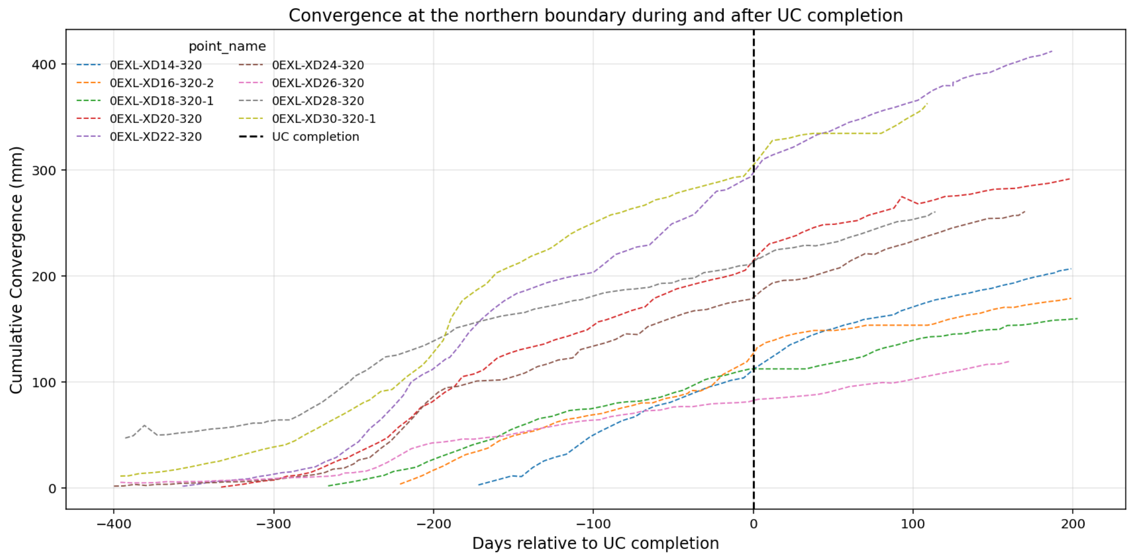

Figure 11 Consistent convergence at the northern boundary during and after undercutting

Instability along the northern boundary reflects the interaction of operational stress evolution and local structural weakness:

- Extended abutment exposure at the end of the undercut sequence led to elevated and prolonged stress concentrations, resulting in earlier onset and higher cumulative convergence.
- Intersection with the Lower Fault and associated damage zone reduced rock mass strength and stiffness, promoting disproportionate deformation in affected pillars during undercutting and pillar formation.
- Early cave loading following UC completion re-accelerated convergence in these already weakened pillars, despite broadly similar post-UC convergence rates across the northern boundary.

This operational–geological coupling explains the spatial clustering of drawpoint pillar damage, and the characteristic deformation-rate signatures observed in the northern boundary pillars.

4 Conclusion

This study demonstrates that elevated deformation and localised damage of EXL drawpoint pillars at OTP0 are driven by the combined effects of prolonged abutment exposure during undercutting and local structural weakening associated with the Lower Fault splay. Northern boundary pillars experienced earlier onset and greater cumulative convergence, with deformation re-accelerated during pillar formation and early caving under increasing cave loading. These behaviours are effectively captured through simple convergence monitoring, supported by consistent trends across independent instrumentation. The findings reinforce key undercut design principles for deep block caves, including undercut initiation in weaker rock mass, control of undercut front length, and management of undercut area in accordance with the evolving stress–strength ratio.

References

Batkhuu, B & van As, A 2026, 'Insight into undercut-induced ground deformations in cave mines', *Deep Resources Engineering,* vol. 3, issue 2, https://doi.org/10.1016/j.deepre.2026.100239

Crane, D & Kavalieris, I 2012, 'Geologic overview of the Oyu Tolgoi porphyry CuAuMo deposits, Mongolia', in JW Hedenquist, M Harris & F Camus (eds), *Geology and Genesis of Major Copper Deposits and Districts of the World: A Tribute to Richard H. Sillitoe* Society of Economic Geologists, https://doi.org/10.5382/SP.16.09

Jakubec, J & Laubscher, DH 2000, 'The MRMR rock mass rating classification system in mining practice', *In Proceedings of the 3rd International Conference and Exhibition on Mass Mining*, Australasian Institute of Mining and Metallurgy, Melbourne, pp. 413–421.

Moorcroft, TH, Simanjuntak, K, Dorjsuren, O, Sanaakhorol, M, Enkhtaivan, E, Watt, G, … & Zimmermann, T 2022, 'Oyu Tolgoi and Rio Tinto partnership with Palantir Technologies to provide effective geotechnical risk management', in Y Potvin (ed.), *Caving*

2022: Proceedings of the Fifth International Conference on Block and Sublevel Caving, Australian Centre for Geomechanics, Perth, pp. 877–890, https://doi.org/10.36487/ACG_repo/2205_60

Ooi, J 2020, *Internal Presentation for Technical Advisory Committee Update,* Oyu Tolgoi LLC.

Ooi, J, Watt, G & Grobler, H 2022, 'Raisebore stability and support at deep depth and highly defected rock mass condition: Oyu Tolgoi case study', in Y Potvin (ed.), *Caving 2022: Proceedings of the Fifth International Conference on Block and Sublevel Caving,* Australian Centre for Geomechanics, Perth, pp. 891–906, https://doi.org/10.36487/ACG_repo/2205_61

Oyu Tolgoi 2025, *Trigger Action Response Plan for Preventive Support Maintenance (PSM), Rehabilitation, and Closure in Footprint Area of P0-P2N Hugo Lift 1 (OT-P0-PSM-TARP).*

Pierce, ME 2018, 'Forecasting vulnerability of deep extraction level excavations to draw-induced cave loads', *Journal of Rock Mechanics and Geotechnical Engineering*, vol. 11, no. 3, pp. 527–534, https://doi.org/10.1016/j.jrmge.2018.07.006

Porter, TM 2016, 'The geology, structure and mineralisation of the Oyu Tolgoi porphyry copper-gold-molybdenum deposits, Mongolia: A review', *Geoscience Frontiers*, vol. 7, no. 3, pp. 375–407, https://doi.org/10.1016/j.gsf.2015.08.003

Russo, A, Cabezas, R & Ramírez, C 2023, *Integrated Geotechnical Characterisation for All Panels – Oyu Tolgoi*, report for SRK Consulting, Santiago.

Wooders, H, de Hennin, S & Bumtseren, S 2024, 'Critical Path analysis and management techniques in development scheduling at Oyu Tolgoi', in D Johansson & H Schunnesson (eds), *MassMin 2024: Proceedings of the International Conference & Exhibition on Mass Mining*, Luleå University of Technology, Luleå, pp. 141–152, https://doi.org/10.36487/ACG_repo/2435_A-13